GEOPHYSICAL RESEARCH LETTERS, VOL. 35, L17602, doi:10.1029/2008GL034687, 2008

Causes of decadal subsurface cooling in the tropical Indian Ocean during 1961–2000

Laurie L. Trenary[1] and Weiqing Han[1]

Received 14 May 2008; revised 24 July 2008; accepted 8 August 2008; published 13 September 2008.

[1] The vertical structure of temperature change in the Indian Ocean (IO) during 1961–2000 indicates that a region of tropical thermocline cooling accompanies the upper level warming. Results from data analysis and ocean general circulation model experiments suggest that the cooling signals exceed the cross-data and cross-model differences. Spatial patterns of the temperature trend above 200 m resemble the negative IO dipole structure, with the strongest cooling occurring in the western-central basin south of the equator. The upper thermocline cooling is mainly caused by enhanced Ekman pumping velocity, which shoals the thermocline. The enhanced upwelling is consistent with the strengthened Southern subtropical cell. Enhanced equatorial westerly winds contribute to the negative dipole pattern. Remote forcing from the Pacific may contribute to the cooling below 200 m and further south. **Citation:** Trenary, L. L., and W. Han (2008), Causes of decadal subsurface cooling in the tropical Indian Ocean during 1961–2000, *Geophys. Res. Lett.*, *35*, L17602, doi:10.1029/2008GL034687.

1. Introduction

[2] Observational evidence for the last few decades suggests that the world ocean is warming, with the strongest warming confined to the upper few hundred meters [*Levitus et al.*, 2005]. The vertical structure of the linear trend of oceanic heat content indicates that regions of cooling accompany the near-surface warming in both the Indian and Pacific Oceans [*Barnett et al.*, 2005; *Han et al.*, 2006; *Intergovernmental Panel on Climate Change*, 2007]. In the Indian Ocean (IO), maximum cooling occurs in the upper thermocline and attains the largest amplitude near 10°S. Several climate models employed for the 20th century experiments of the Intergovernmental Panel on Climate Change [*Intergovernmental Panel on Climate Change*] documented thermocline cooling signals of the tropical-subtropical IO [e.g., *Alory et al.*, 2007; *Cai et al.*, 2008].

[3] Attempts have been made recently to explain the development of the IO subsurface cooling. *Han et al.* [2006] used a simple 2-layer equilibrium state model and suggested that cooling in the upper thermocline during 1960–1999 is primarily associated with anomalous upward Ekman pumping velocities over the IO. In contrast, *Alory et al.* [2007] suggests that cooling of the south IO is remotely forced by a shoaling of the western Pacific equatorial thermocline, which is transmitted to the IO by the Indonesian Throughflow (ITF). Note that the ITF may also affect the IO thermocline through thermal advection. Other possible mechanisms may also cause thermocline anomalies: spin up or spin down of the subtropical cells (STCs) [e.g., *Liu*, 1994; *McCreary and Lu*, 1994; *McPhaden and Zhang*, 2002], mid-latitude cooling/warming [*Huang and Pedlosky*, 2000; *Boccaletti et al.*, 2004] and influence from the Antarctic Circumpolar Current (ACC). How the ACC affects the IO thermocline remains unknown. As a first step, we begin by examining the variability of the IO winds and STCs in relation to the subsurface cooling trend.

[4] It is suggested that the strength of the STC is controlled by the zonal wind stress at the latitude where the Ekman pumping velocity equals zero [*McCreary and Lu*, 1994; *Liu*, 1994]. On decadal or longer time scales, the STC is assumed to be quasi-steady [e.g., *McCreary and Lu*, 1994]. Consequently, enhanced tropical upwelling should be compensated by enhanced meridional transport of the STC. Modeling and observational studies, primarily focused on the equatorial Pacific, have provided support for the effects of STCs on equatorial temperature [e.g., *Kleeman et al.*, 1999; *McPhaden and Zhang*, 2002]. In the IO, the shallow meridional overturning circulations consist of the southern STC (SSTC) and Cross-Equatorial Cell (CEC) [*Schott et al.*, 2004; *Lee*, 2004]. The SSTC (CEC) involves a wind-driven southward surface flow and a compensating equatorward thermocline flow, which connect the upwelling region of the south tropical IO near 2°S–12°S (north IO) [*Murtugudde et al.*, 1999; *Xie et al.*, 2002] to the subduction zone of the south subtropical IO [*Schott et al.*, 2004]. If the northward transport of the subducted water from the subtropics to the tropics remains the same, a weakened CEC will accompany an enhanced SSTC.

2. Data and Models

[5] The annual mean gridded data from the World Ocean Database 2005 (WOD05) [*Levitus et al.*, 2005], and monthly data from the Simple Ocean Data Assimilation using Parallel Ocean Program (SODA-POP) [*Carton and Giese*, 2008] for the period of 1961–2000 are analyzed. This period of time is chosen because the SODA-POP forcing fields, the ECMWF 40-year reanalysis (ERA40) data, are available.

[6] An experiment was performed using the HYbrid Coordinate Ocean Model (HYCOM) [*Bleck*, 2002] for the Indo-Pacific basin (40°S–55°N), with a horizontal resolution of 0.5° × 0.5° and 22 vertical levels. Near the southern boundary, HYCOM temperature and salinity fields are relaxed to Levitus climatology. After spin-up, the model was integrated forward using 3-day-mean ERA40 fields for the period of 1958–2001. Solutions to the global POP

[1]Department of Atmospheric and Oceanic Sciences, University of Colorado, Boulder, Colorado, USA.

0094-8276/08/2008GL034687$05.00

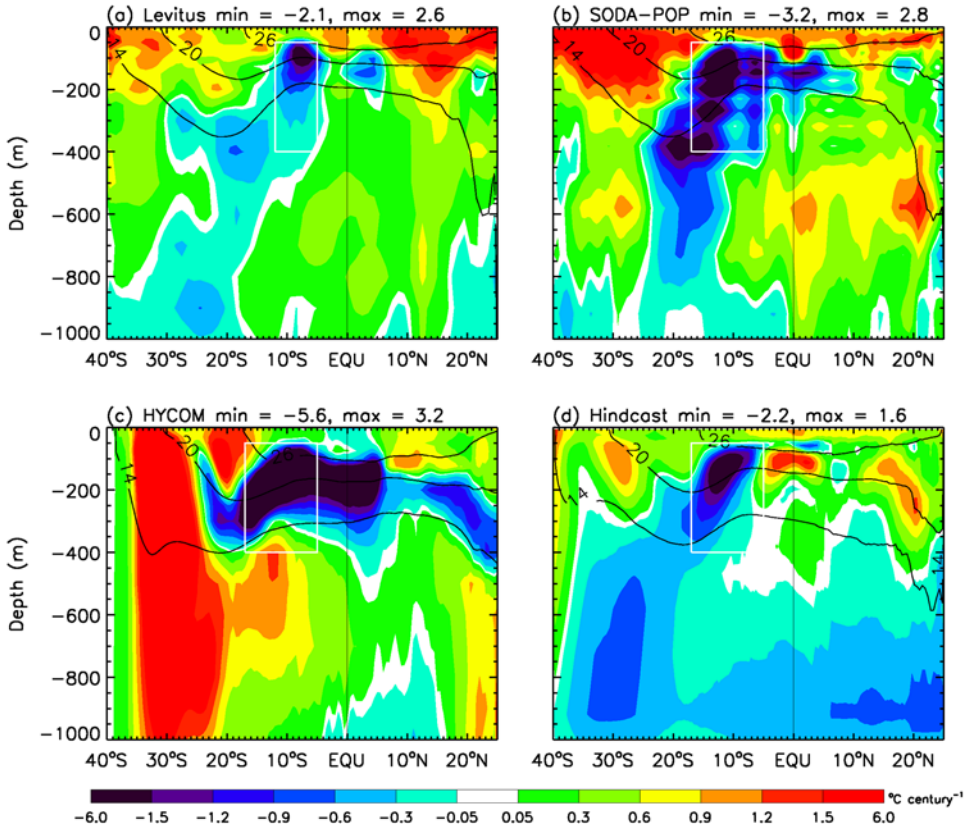

Figure 1. Latitude-depth plot of linear trend of temperature zonally-averaged over the IO from (a) WOD05, (b) SODA-POP, (c) HYCOM, and (d) POP-Hindcast during 1961–2000. The black contours show the mean 26°, 20° and 14°C isotherms from the 1960's. White boxes are used to define trend indexes in Figure 2d.

1.4.3, the ocean component of the National Center for Atmospheric Research (NCAR) Community Climate System Model, are also analyzed. The model was forced by the National Center for Environmental Prediction (NCEP) – NCAR reanalysis from 1958–2000 [*Doney et al.*, 2007].

3. Results

3.1. Temperature Variability

[7] A cooling trend in the tropical IO thermocline for the period of 1961–2000 is shown in all four datasets, in addition to surface warming. Both the WOD05 and SODA-POP data (Figures 1a and 1b) show that the warming between 5°N–15°S is trapped to the surface and caps a region of thermocline cooling, with the strongest cooling mainly occurring above 200 m, SODA-POP data shows an additional region of strong cooling near 400 m. Weaker cooling signals, found in both datasets, extend downward and southward at greater depths.

[8] HYCOM captured the strong cooling in the upper thermocline and the near-surface warming (Figure 1c). The cooling region, however, shows little extent into the deeper ocean below 400 m. Cooling in the north IO is also stronger than the WOD05 and SODA-POP data. These model/data discrepancies are likely due to the artificial boundary at 40°S, which excludes subduction that occurs further south, does not allow the return flow south of Australia and excludes the effects of ACC. POP-Hindcast also shows cooling of the upper thermocline south of the equator (Figure 1d). Relative to WOD05 and SODA-POP data, the cooling extends too far south in the deeper layers. The lower thermocline cooling of the northern hemisphere also disagrees with the warming from other datasets. Nevertheless, cooling in the thermocline above 400 m – which is the focus of this paper – is shown in both data and model solutions.

[9] The spatial structure of the linear trend of temperature is illustrated in Figures 2a–2c for 70∼75 m from HYCOM, SODA-POP and POP-Hindcast. Albeit with quantitative differences, all data show a strong cooling trend south of the equator especially in the central-western basin, weaker cooling north of the equator in the central ocean and warming in the eastern tropical basin, a pattern that qualitatively resembles the IO dipole (IOD) [e.g., *Saji et al.*, 1999; *Webster et al.*, 1999]. The consistent thermocline cooling trends south of the equator from all datasets are also shown in Figure 2d, which corresponds to a trend toward a negative IOD.

[10] The dipole pattern is well captured by the first empirical orthogonal function (EOF1) of temperature variability (compare Figures 2e and 2a), and is also shown at 125 m (Figure 2f). The first 4 EOF modes explain about 37% of the total variance at 75 meters, with EOF1 accounting for 15%. At 125 m, the first 4 modes explain about 45% of the total variance, with EOF1 accounting for 19%. The dipole pattern disappears at 200 m, and the EOF1 shows a

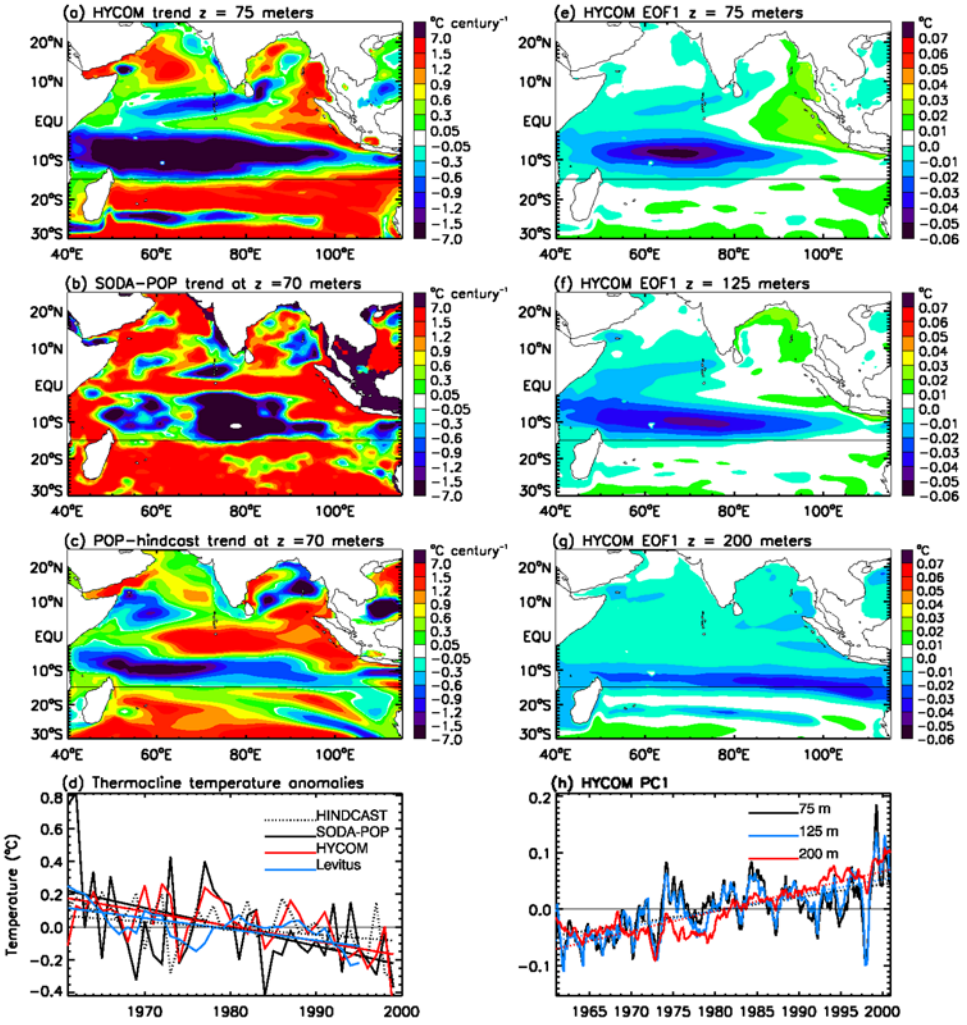

Figure 2. (a) Spatial pattern of temperature linear trend at 75 m from HYCOM solution; (b) Same as Figure 2a except for SODA-POP temperature trend; (c) Same as Figure 2a except for POP-Hindcast temperature trend; (d) Time series of the thermocline temperature anomaly averaged over the cooling region (white boxes in Figure 1) for WOD05 (blue), HCYOM (red), POP-Hindcast (dotted), and SODA-POP (black); (e, f, g) first EOF of temperature variability from HYCOM solution at 75 m, 125 m and 200 m; (h) Time series of the principle component (PC) associated with the first EOFs at 75, 125 and 200 m.

monopole structure (Figure 2g). The principle components (PCs) for each of the leading EOFs (Figure 2h) collectively show trends toward a cooling phase in the southern tropical IO, which again corresponds to a trend toward a negative IOD. It is also clearly evident that temperature in the upper-thermocline shows strong interannual-to-decadal scale variability (black and blue lines of Figure 2h).

[11] HYCOM solutions show that the strongest cooling in the central-western basin in the upper-thermocline extends eastward with the increase of depth, with maximum cooling occurring near the ITF region at 200 m (Figures 2e–2g). Linear trend of the 20°C isotherm depth (D20) shows weak connection with the ITF (see auxiliary Figure S1[1]). Analysis of WOD05 and SODA-POP data similarly indicate that shoaling of the upper thermocline is greatest in the central-western basin, while the POP-Hindcast solution shows a more pronounced connection to the ITF region at all depths (not shown). The strong cooling near the ITF region at 200 m (Figure 2g) and below (not shown) may suggest the contribution from the western equatorial Pacific via wave transmission, although it can also be contributed from local wind forcing.

3.2. IO STC Variability and Winds

[12] Figure 3a (black curve) shows the time series of the estimated strength of the STC, given by the meridional Ekman transport computed from the ERA40 winds at 15°S, the latitude where Ekman pumping velocity $W_e \sim 0$ (not shown). In the IO, this estimate measures the total strength of the SSTC and CEC [*Schott et al.*, 2004; *Lee*, 2004]. The southward Ekman transport has an increasing trend and enhances by ~2 Sverdrup (Sv) from 1961–2000. Consis-

[1]Auxiliary materials are available in the HTML. doi:10.1029/2008GL034687.

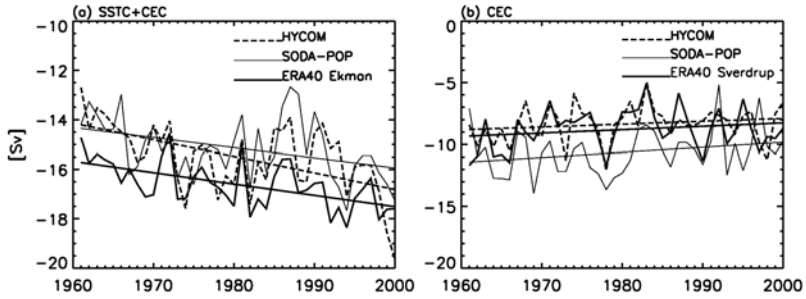

Figure 3. (a) Time series of the upper-layer southward transport in HYCOM (dashed line), SODA-POP (thin line) and the Ekman transport computed from ERA40 winds (thick line) at 15°S; the ERA40 winds are used to force both SODA-POP and HYCOM. (b) The upper-layer southward transport at the equator in HYCOM (dashed line), SODA-POP (thin) and the Sverdrup transport computed from ERA40 winds (thick line). The upper layer transport in HYCOM is the zonal integral of meridional transport from 48°E–115°E at 15°S in the layers equal and above 22.25 kgm^{-3} (below which transport reverses), and from 46°E–100°E at the equator in the layers equal and above 26.18 kgm^{-3}. The upper-layer transports in SODA-POP were computed over the same longitudinal bands, from the surface to the depth where transport reverses.

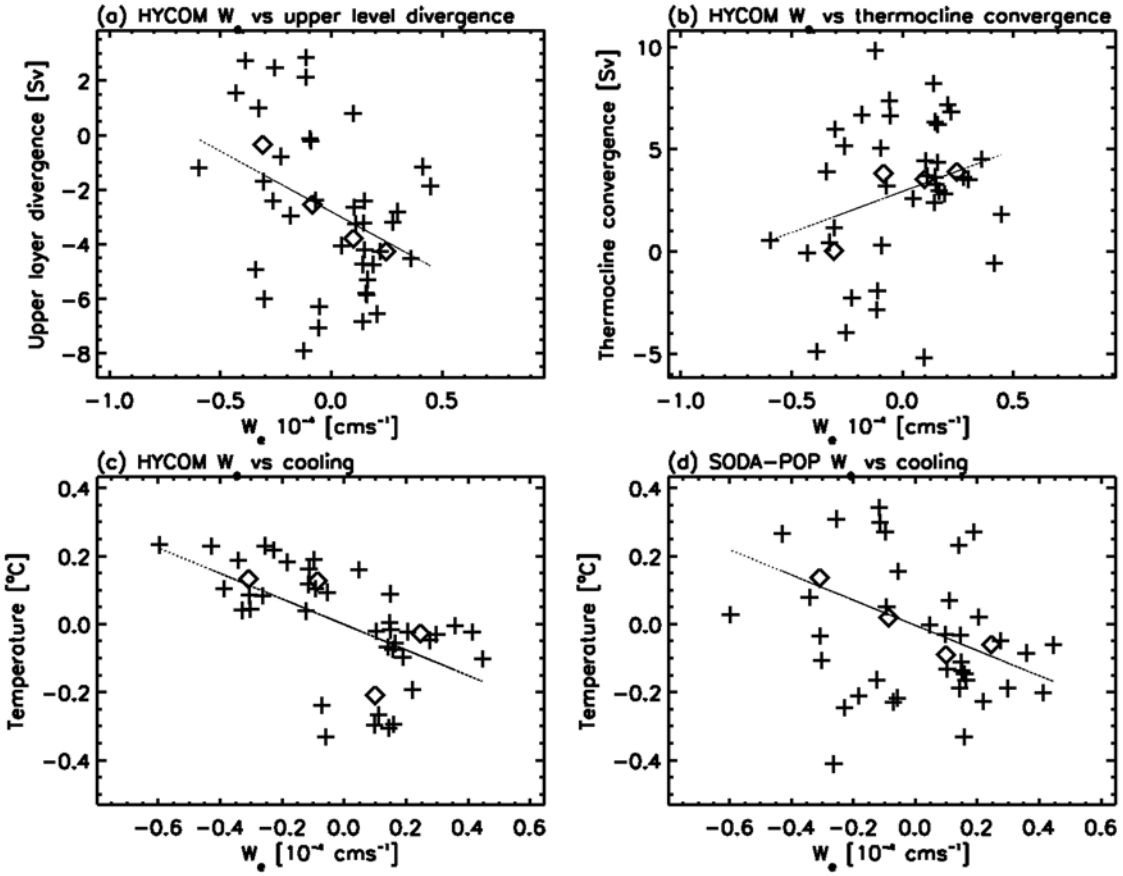

Figure 4. (a) A scatter plot of upper-layer divergence between 15°S–0°S in HYCOM versus W_e anomaly calculated from the ERA40 winds averaged over 15°S–3°S. (b) Same as Figure 4a except for thermocline convergence versus W_e anomaly. (c) Same as Figure 4a except for thermocline temperature anomaly averaged in the white box of Figure 1c versus W_e anomaly. (d) Same as Figure 4c except for SODA-POP thermocline temperature anomaly versus W_e anomaly. Annual mean values denoted by crosses. Decadal mean values denoted by diamonds. The thermocline convergence is the difference between the thermocline transport at 15°S and transport of the western boundary current at 0°N (see *Schott et al.* [2004] for CEC pathways). The thermocline transport at 15°S is the zonal integral of meridional transport from 48°E–115°E for layers 23.25–26.18 kgm^{-3}, and along the equator from 35°E–46°E for layers equal and above 26.18 kgm^{-3}.

tently, the southward upper-level transports from both SODA-POP and HYCOM increase by 2∼3 Sv (Figure 3a).

[13] Interestingly, while the total transport associated with the SSTC and CEC is strengthening, the CEC individually spins down (Figure 3b). The spin down of the CEC is consistent with the estimate of *Schoenefeldt and Schott* [2006]. The difference between the enhanced southward transport at 15°S and the weakened CEC suggests a surface divergence of ∼3–4 Sv within the 15°S–0°S band, indicating that the SSTC enhances by 3∼4 Sv. This latitudinal band is the upwelling zone of the SSTC and in conjunction is the region of strongest cooling and enhanced W_e.

[14] Figures 4a and 4b show scatter plots of the annual mean surface-layer divergence and thermocline-layer convergence between 15°S–0°S from HYCOM solutions in relation to the annual and zonal mean W_e anomaly averaged over 15°S–3°S. Of particular interest is the high degree of correlation between the spin up of the SSTC and enhanced W_e on decadal time scales, indicating that the quasi-steady assumption of the STC on decadal timescale may be valid. A correlation on interannual time scales is not apparent. In turn, the enhanced W_e is highly correlated with the thermocline cooling on decadal timescales in both the HYCOM solution and SODA-POP data (Figures 4c and 4d). The enhanced W_e corresponds to progressive cooling of the thermocline. These results suggest that a relationship exists between the enhanced W_e, spin-up of the SSTC and thermocline cooling. In addition, the enhanced equatorial westerly winds found in both ERA40 and NCEP reanalysis (not shown) contribute to the anomalous warming in the eastern equatorial basin and cooling in the off equatorial central-western basin, through anomalous equatorial Ekman convergence and off-equatorial Ekman divergence. This contributes to the negative IOD trend shown in Figure 2.

4. Discussion

[15] Spatial patterns of IO subsurface temperature variability show that the maximum upper level cooling is located in the western-central basin of the south IO. At greater depths, the maximum cooling appears to extend from the Indonesian passage, suggesting that more apparent, direct influence of the ITF on the thermocline variability of the south IO might be below 200 m. It is quite possible that both local forcing of the IO and remote forcing from the Pacific via the ITF have contributed to the enhanced subsurface cooling. Elucidation of the ITF influence on the subsurface heat budget is beyond the scope of this work, but is certainly an area of ongoing research.

[16] The dipole structure of the thermocline temperature trend is associated with enhanced equatorial westerlies and strengthened southeasterly trades in the south IO, which in turn result in enhanced W_e in the upwelling zone of the SSTC. The enhanced W_e is consistent with the shoaling thermocline and spin up of the SSTC, which increased by 3∼4 Sv from 1961 to 2000 and is strongly correlated with the thermocline cooling on decadal timescale.

[17] **Acknowledgments.** The authors are supported by NSF OCE 0452917 and NASA Ocean Vector Wind Science Team award 1283568. We gratefully acknowledge the Oceanography section at NCAR for making the POP-Hindcast data available. We thank ECMWF and NCAR for the ERA40 fields, Balaji Rajagopalan for his guidance on EOF analysis, and an anonymous reviewer for helpful and insightful comments.

References

Alory, G., S. Wijffels, and G. A. Meyers (2007), Observed temperature trends in the Indian Ocean over 1960–1999 and associated mechanisms, *Geophys. Res. Lett.*, *34*, L02606, doi:10.1029/2006GL028044.

Barnett, T. P., D. W. Pierce, K. M. AchutaRao, P. J. Gleckler, B. D. Santer, J. M. Gregory, and W. M. Washington (2005), Penetration of human-induced warming into the world's oceans, *Science*, *309*, 284–287.

Bleck, R. (2002), An oceanic general circulation model framed in hybrid isopycnic-Cartesian coordinates, *Ocean Modell.*, *4*, 55–88.

Boccaletti, G., R. C. Pacanowski, S. G. H. Philander, and A. V. Fedorov (2004), The thermal structure of the upper ocean, *J. Phys. Oceanogr.*, *34*, 888–902.

Cai, W., A. Sullivan, and T. Cowan (2008), Shoaling of the off-equatorial south Indian Ocean thermocline: Is it driven by anthropogenic forcing?, *Geophys. Res. Lett.*, *35*, L12711, doi:10.1029/2008GL034174.

Carton, J. A., and B. Giese (2008), A reanalysis of ocean climate using SODA, *Mon. Weather*, in press.

Doney, S., S. Yeager, G. Danabasoglu, W. Large, and J. C. McWilliams (2007), Mechanisms governing interannual variability of upper-ocean temperature in a global ocean hindcast simulation, *J. Phys. Oceanogr.*, *37*, 1918–1938.

Han, W., G. A. Meehl, and A. Hu (2006), Interpretation of tropical thermocline cooling in the Indian and Pacific oceans during recent decades, *Geophys. Res. Lett.*, *33*, L23615, doi:10.1029/2006GL027982.

Huang, R. X., and J. Pedlosky (2000), Climate variability of the equatorial thermocline inferred from a two-moving-layer model of the ventilated thermocline, *J. Phys. Oceanogr.*, *30*, 2610–2626.

Intergovernmental Panel on Climate Change (2007), *Climate Change 2007— The Physical Science Basis, Contribution of Working Group I to the Forth Assessment Report of the IPCC*, Cambridge Univ. Press, New York.

Kleeman, R., J. P. McCreary, and B. Klinger (1999), A mechanism for generating ENSO decadal variability, *Geophys. Res. Lett.*, *26*, 1743–1746.

Lee, T. (2004), Decadal weakening of the shallow overturning circulation in the South Indian Ocean, *Geophys. Res. Lett.*, *31*, L18305, doi:10.1029/2004GL020884.

Levitus, S., J. Antonov, and T. Boyer (2005), Warming of the world ocean, 1955–2003, *Geophys. Res. Lett.*, *32*, L02604, doi:10.1029/2004GL021592.

Liu, Z. (1994), A simple model of the mass exchange between the subtropical and tropical ocean, *J. Phys. Oceanogr.*, *24*, 1153–1165.

McCreary, J. P., and P. Lu (1994), Interaction between the subtropical and equatorial ocean circulations: The subtropical cell, *J. Phys. Oceanogr.*, *24*, 466–497.

McPhaden, M. J., and D. Zhang (2002), Slowdown of the meridional overturning circulation in the upper Pacific Ocean, *Nature*, *415*, 603–608.

Murtugudde, R., et al. (1999), Ocean color variability of the tropical Indo-Pacific basin observed by SeaWiFS during 1997–1998, *J. Geophys. Res.*, *104*, 18,351–18,366.

Saji, N. H., B. N. Goswami, P. N. Vinayachandran, and T. Yamagata (1999), A dipole mode in the tropical Indian Ocean, *Nature*, *401*, 360–363.

Schoenefeldt, R., and F. Schott (2006), Decadal variability of the Indian Ocean cross-equatorial exchange in SODA, *Geophys. Res. Lett.*, *33*, L08602, doi:10.1029/2006GL025891.

Schott, F., J. P. McCreary, and G. C. Johnson (2004), Shallow overturning circulations of the tropical-subtropical oceans, in *Earth's Climate: The Ocean-Atmosphere Interaction, Geophys. Monogr. Ser.*, vol. 147, edited by C. Wang, S.-P. Xie, and J. A. Carton, pp. 261–304, AGU, Washington, D. C.

Webster, P. J., A. M. Moore, J. P. Loschnigg, and R. R. Leben (1999), Coupled ocean-atmosphere dynamics in the Indian Ocean during 1997–-1998, *Nature*, *401*, 356–360.

Xie, S.-P., H. Annamalai, F. A. Schott, and J. P. McCreary (2002), Structure and mechanisms of south Indian Ocean climate variability, *J. Clim.*, *15*, 864–878.

W. Han and L. L. Trenary, Department of Atmospheric and Oceanic Sciences, University of Colorado, UCB 311, Boulder, CO 80309, USA. (laurie.trenary@.colorado.edu)